Author Manuscript

Author Manuscript

Author Manuscript

Author Manuscript

HHS Public Access

Author manuscript

Genet Med. Author manuscript; available in PMC 2021 September 17.

Published in final edited form as:

Genet Med. 2021 July ; 23(7): 1305–1314. doi:10.1038/s41436-021-01137-6.

Lysosomal Cholesterol Accumulation Contributes to the Movement Phenotypes Associated with *NUS1* Haploinsufficiency

Seok-Ho Yu[1], **Tong Wang**[1], **Kali Wiggins**[1], **Raymond J. Louie**[1], **Emilio F. Merino**[2], **Cindy Skinner**[1], **Maria B. Cassera**[2], **Kirsten Meagher**[3], **Paul Goldberg**[3], **Neggy Rismanchi**[4], **Dillon Chen**[4], **Michael J. Lyons**[1], **Heather Flanagan-Steet**[1], **Richard Steet**[#,1]

[1]Greenwood Genetic Center, Greenwood, SC 29646

[2]Department of Biochemistry and Molecular Biology, and Center for Tropical and Emerging Global Diseases (CTEGD), University of Georgia, Athens, GA 30602

[3]Department of Medical Genetics, British Columbia Women's Hospital and Health Centre, Vancouver, BC V6H 3N1

[4]Department of Neuroscience at the University of California, San Diego, San Diego, California 92093; Division of Neurology, Rady Children's Hospital San Diego, San Diego, California, 92123

Abstract

Users may view, print, copy, and download text and data-mine the content in such documents, for the purposes of academic research, subject always to the full Conditions of use:http://www.nature.com/authors/editorial_policies/license.html#terms

[#]corresponding author: Richard Steet, PhD, JC Self Research Institute, Greenwood Genetic Center, 113 Gregor Mendel Circle, Greenwood, SC 29646 USA, Tel: +001- 864-3881807.

Author Contributions

Conceptualization: R.S., H.F-S., M.J.L.; Data curation: S.Y., T.W., E.F.M., M.B.C., R.J.L., H.F-S., R.S.; Formal analysis: S.Y., T.W., R.J.L., H.F-S., R.S.; Funding acquisition: R.S., H.F-S., M.B.C.; Investigation: S.Y., T.W., K.W., R.J.L., E.F.M., H.F-S.; Methodology: S.Y., T.W., M.B.C., H.F-S., R.S.; Project Administration: R.S., H.F-S., M.J.L.; Resources: C.S., K.M., P.G., N.R., D.C., M.J.L.; Supervision: R.S., H.F-S.; Validation: T.W., H.F-S.; Visualization: S.Y., T.W., H.F-S.; Writing- original draft: R.S., H.F-S., M.J.L., R.J.L.; Writing- review & editing: R.S., H.F-S.

Conflict of Interest Statement

All the authors declare that they have no competing or financial conflicts of interest.

Declaration of interests

The authors declare no competing interests.

Data and code availability

All variants described in this study have been deposited in ClinVar; accession numbers are VCV000981036, VCV000981034, VCV000981035 (Submission ID: SUB8124960; Organization ID: 1019)

Provean (protein variation effect analyser), http://provean.jcvi.org/index.php
PolyPhen2, http://genetics.bwh.harvard.edu/pph2/;
MutationTaster, http://mutationtaster.org/
dbSNP, https://www.ncbi.nlm.nih.gov/snp/
gnomAd, http://gnomad.broadinstitute.org/
Mutalyzer, https://mutalyzer.nl/batch-jobs
ClinVar, https://www.ncbi.nlm.nih.gov/clinvar/

Ethics statement

Informed consents were signed by the parents of the proband and other patients prior to participation in the research. All procedures were employed after being reviewed and approved by the Institutional Review Board, and compliant with practices at the Greenwood Genetic Center (GGC). Handling and euthanasia of fish complied with policies of the GGC, as approved by the GGC's Institutional Animal Care and Use Committee (permit #A2019-01-003-A1).

Author Manuscript Author Manuscript Author Manuscript Author Manuscript

Purpose: Variants in *NUS1* are associated with a congenital disorder of glycosylation, developmental and epileptic encephalopathies, and are possible contributors to Parkinson's disease pathogenesis. How the diverse functions of the *NUS1*-encoded Nogo B receptor (NgBR) relate to these different phenotypes is largely unknown. We present three patients with *de novo* heterozygous variants in *NUS1* that cause a complex movement disorder, define pathogenic mechanisms in cells and zebrafish, and identify possible therapy.

Methods: Comprehensive functional studies were performed using patient fibroblasts, and a zebrafish model mimicking *NUS1* haploinsufficiency.

Results: We show that *de novo NUS1* variants reduce NgBR and Niemann-Pick type C2 (NPC2) protein amount, impair dolichol biosynthesis, and cause lysosomal cholesterol accumulation. Reducing *nus1* expression 50% in zebrafish embryos causes abnormal swim behaviors, cholesterol accumulation in the nervous system and impaired turnover of lysosomal membrane proteins. Reduction of cholesterol buildup with 2-hydroxypropyl-ß-cyclodextrin significantly alleviates lysosomal proteolysis and motility defects.

Conclusions: Our results demonstrate that these *NUS1* variants cause multiple lysosomal phenotypes in cells. We show that the movement deficits associated with *nus1* reduction in zebrafish arise in part from defective efflux of cholesterol from lysosomes, suggesting that treatments targeting cholesterol accumulation could be therapeutic.

Introduction:

NUS1, located on 6q22.1, encodes the Nogo B receptor (NgBR), a highly conserved multifunctional protein. NgBR associates with the *DHDDS* gene product (CIT; cis-isoprenyltransferase), to form a heterodimeric complex with cis-prenyltransferase activity [1-4]. This complex is necessary for the biosynthesis of polyprenol and dolichol lipids, with the latter serving as the lipid carrier for precursors of the N-linked glycosylation pathway [5]. The C-terminus of NgBR also interacts with and stabilizes NPC2, the soluble lysosomal protein required for proper efflux of cholesterol out of lysosomes to the ER [6]. Lastly, NgBR is the receptor for Nogo-B, a ligand that is highly expressed in the vasculature and facilitates the chemotaxis and adhesion of endothelial cells [7-9].

The relevance of this gene to human health was recently highlighted by the identification of *NUS1*-CDG (OMIM #617082) patients bearing pathogenic homozygous variants in this gene [10]. Fibroblasts from these patients displayed defects in N-glycosylation and intralysosomal cholesterol storage resembling pathogenic variants in the *NPC1* and *NPC2* genes. Individuals with *de novo*, heterozygous, loss-of-function variants in *NUS1* have also been reported in association with autosomal dominant type 55 intellectual disability with seizures (OMIM #617831) [11]. *NUS1* is also a proposed contributor to Parkinson's disease (PD), as an increased frequency of missense variants within this gene have been observed in patients with early onset PD [12; 13]. More recent studies, however, draw this connection into question [12; 14; 15]. Other genetic studies have found *de novo NUS1* variants in patients with complex dystonia, ataxia, tremor and epilepsy, reinforcing the biological importance of this gene in neuronal and/or neuromuscular systems [16-19]. Despite the growing number of patients with movement phenotypes bearing *NUS1* variants, the mechanistic basis for these

Author Manuscript Author Manuscript Author Manuscript Author Manuscript

phenotypes is largely lacking. Moreover, it is not known whether these reported heterozygous variants cause glycosylation and/or lysosomal defects in patient cells.

Here we report three patients bearing *de novo*, heterozygous *NUS1* variants that present with a range of neurological manifestations and movement phenotypes. Functional studies in two of the patient cell lines revealed a spectrum of lysosomal-related defects consistent with the functions mediated by NgBR. Knockdown of *nus1* in zebrafish caused altered swimming behaviors, neuronal cholesterol storage, and impaired turnover of a lysosomal integral membrane protein. Congruent with a role for intracellular cholesterol accumulation in the development of these phenotypes, treatment of *nus1*-depleted embryos with 2-hydroxypropyl-ß-cyclodextrin significantly improved the phenotypic and molecular consequences. These findings provide insight into the mechanistic basis for the movement phenotypes associated with heterozygous *NUS1* variants. The implications of these results with regard to the mechanistic basis and clinical management of the neurological manifestations in these patients is discussed.

Materials and Methods:

The methods for cell-based analyses are found in the Supplementary files.

Biochemical experiments in zebrafish:

For Western blots, embryos were manually deyolked and harvested at the time points indicated. Protein concentration in detergent lysates was determined using the micro-BCA assay. The primary antibodies included anti-NgBR (Abcam, ab168351, 1:500), anti-NPC2 (1:1000, R&D Systems, AF8644) and anti-Cherry (cat# ab167453, Abcam). Western blots were developed using Clarity Western ECL Substrate (BioRad) and analyzed on the Bio-Rad ChemiDoc Imaging System. For Western analyses of Lamp1 following heat shock, 4dpf embryos were incubated in 39°C embryo water for 30 minute to induce expression. Embryos were subsequently harvested at the indicated time points post heat shock. For filipin staining, 6-7dpf embryos were fixed with 4% paraformaldehyde at 4°C overnight. Fixed embryos were rinsed with phosphate buffered saline and stained with 0.5mg/mL of filipin (Sigma, F4767-1MG) and 1% goat serum for 2.5 hours at room temperature. Stained embryos were mounted in 0.8% hanging agarose drops. Embryos were imaged with a 40X water immersion objective (N.A.1.15) on an Olympus FV3000 laser scanning confocal microscope. For treatment with 2-hydroxypropyl-beta-cyclodextrin (ßCD, Sigma, SLBX3717), 100mM stock solution was generated in water. Embryos were treated at time points indicated by adding ßCD at a final concentration of 2.5 mM to their growth medium. Projections were generated using the Image J software (NIH) and processed using Adobe PhotoShop (CS6).

Antisense morpholino injections and ZebraBox:

Morpholino knockdown of *nus1* was performed using a previously validated translation-blocking morpholino (5′-ACACCATCTCATACAGCGAAGCCAT-3′) was purchased from Gene Tools, LLC (Eugene. OR). The degree of morpholino knockdown was assayed by Western blot using the anti-NgBR antibody following injection of 0.3-1.0μM reagent into 1-

Author Manuscript Author Manuscript Author Manuscript Author Manuscript

cell stage embryos. 4-5dpf, larvae were placed one per well into 12-well plates containing 2 mls embryo medium. T Locomotor activity was monitored 5-8dpf using the Zebrabox System (ViewPoint Inc., Toronto, Canada). Plate was placed into the sensory deprivation chamber, desensitized for 15 minutes, and behavior subsequently recorded at 10 minute intervals. The low detection threshold was set to 20. The large activity threshold was set to 8 and the inactive threshold was set to 4. Data was analyzed using GraphPad Prizm.

Results:

Clinical description of patients-

The clinical features and exome sequencing results of the patients are summarized in Supplemental Table 1. The technical details of exome sequencing analysis of the different variants for pathogenicity are provided in Supplemental Tables 2 and 3, respectively. The position of these variants within the protein and gene structures is depicted in Supplemental Figure 1.

Patient 1 –

Patient 1 is a now 14-year-old female who presented for a genetics evaluation at age 12 due to concerns for possible spinocerebellar ataxia. She was noted to have a history of borderline intellectual disability, seizures, cerebellar intention tremor, ocular flutter, and mild gait ataxia. Early developmental milestones were normal. She has learning difficulties in school and is noted to be 3-4 grades behind her peers with a full-scale IQ of 76. She has had two major motor seizures along with occasional prolonged absence seizures. Her tremor was first noted at 3 years old and is stable. Ocular movements consist of her eyes moving horizontally back and forth with occasional upward movements. She had a fine tremor with mild gait ataxia and difficulty with tandem walking. Reflexes were normal. She has a normal brain MRI. EEGs revealed mild generalized background slowing with frequent, often low voltage and poorly formed, bifrontal sharp wave discharges occurring in isolation or as runs of 2.5 Hz during sleep. She had normal autosomal dominant and autosomal recessive ataxia gene panels, as well as a normal serum transferrin test. Exome sequencing revealed a *de novo* heterozygous c.734G>T (p.Gly245Val) variant in the *NUS1* gene.

Patient 2 –

Patient 2 is a 35-year-old female who was initially evaluated at 30 years old with a history of moderate intellectual disability, seizures, tremor and slight gait ataxia. Early developmental milestones were delayed with her ability to say single words starting at 3 years old and phrases at 5 years old. She had an initial absence seizure at 4 years old in which she went limp and was unresponsive. She had no subsequent seizures until she had a grand mal seizure at 14 years old. She had three seizures between 14 and 30 years old, all related to medication changes. At 22 years old, she developed a tremor in her hands and feet. An EEG at 28 years old showed left cortical irritation with bursts of spikes, excessive slowing bilaterally and bursts of irregular delta slowing bilaterally. She had a normal brain MRI at 31 years old. Exome sequencing identified a *de novo* heterozygous c.752T>G (p.Leu251*) variant in the *NUS1* gene.

Author Manuscript Author Manuscript Author Manuscript Author Manuscript

Patient 3 –

Patient 3 is a now 5-year-old male who had a genetics evaluation at 3 years old for a history of developmental delay, seizures, and tremor. He has mild to moderate motor delays related to balance issues and moderate to severe speech delay. Seizure activity began at 2 years old with a generalized tonic-clonic seizure associated with fever. He has a history of myoclonic seizures and has more recently developed complex partial seizures which occur a few times a week to multiple times in a day, especially on warmer days. A tremor involving his upper extremities developed at 2 years old. The tremor is worse after seizure activity but improved after treatment with topiramate. He has not developed ataxia but was noted to have dysarthria. No evidence of hypotonia or other neurologic findings were identified. Subcortical parietal gliosis was noted on a brain MRI. EEG revealed abnormal bifrontal or generalized epileptiform discharges. Exome sequencing revealed a *de novo* heterozygous c.415+1G>A variant in the *NUS1* gene.

Functional studies on patient fibroblasts-

In order to define the molecular consequences of the *NUS1* variants, two patient fibroblast lines (from P1 and P2) were used to investigate potential glycosylation defects, intralysosomal cholesterol storage, and the impact of variants on NgBR protein levels. Western blot analysis revealed a 50% reduction in the steady-state level of NgBR protein in both patient cell lines (Figure 1A), supporting the likelihood these variants cause loss of function either through altered transcript abundance or decreased protein stability. Quantitative RT-PCR of P1 cells showed a 30% reduction in *NUS1* transcript abundance (Figure 1B). Cloning and sequencing of amplicons indicate 64% of P1's *NUS1* mRNA is WT, while 36% contains the variant. In P2 cells no reduction in *NUS1* transcript abundance was noted and 58% of the mRNA was WT. However, P2 generates a premature termination codon at position 251 and gel-based analyses of transcripts revealed a shorter species, indicating aberrant mRNA may be degraded by nonsense-mediated decay. A lower molecular weight band also observed in the NgBR Western blot likely represents the truncated protein (Figure 1A). The recently published crystal structures of the *NUS1* and *DHDDS* gene products suggest the substitution of valine for glycine at position 245 in P1 likely disrupts the stability/folding of three ß-sheet structures that converge near that position (Supplemental Figure 2) [1; 2]

To address the functional consequences of the *NUS1* variants, we first asked whether the reduction in NgBR is sufficient to decrease polyprenol/dolichol abundance in patient cells. Lipid analysis was performed on control and patient fibroblasts. The levels of total polyprenol and dolichol lipids were diminished (Figure 1C) in both patient fibroblast lines, suggesting that a 50% reduction in NgBR protein is sufficient to impact biosynthesis of these precursors. Next, possible glycosylation and lysosomal phenotypes were assessed. Western blot for several glycoprotein markers, including an integral lysosomal membrane protein (LAMP2) and the cell adhesion molecule (ICAM1), demonstrated either increased electrophoretic mobility or reduced abundance in the patient cells (Figure 1D; Supplemental Figure 3A). The lack of significant shift in electrophoretic mobility of cellular LAMP2 protein and normal serum transferrin profiles do not support biosynthetic glycosylation defects in these patients. The reduction in ICAM1 abundance in patients' cells is interesting

Author Manuscript Author Manuscript Author Manuscript Author Manuscript

though it is not a specific finding and can be related to other NgBR-related mechanism. Furthermore, qPCR analyses also showed no increase in transcript abundance of multiple ER stress genes in patient cells, suggesting a stress response due to abundant protein underglycosylation is not present (Supplemental Figure 3B).

Association between NgBR and the lysosomal protein NPC2 has been shown to stabilize NPC2, in turn modulating intracellular cholesterol transport and homeostasis [6]. Western blot analysis showed that the steady-state levels of NPC2 were decreased in both patient lines compared to control fibroblasts, with P2 fibroblasts more strongly impacted (Figure 1E). The reductions in NPC2 correspond with increased accumulation of lysosomal cholesterol, as assessed by filipin staining. Although the reduction in NPC2 is less pronounced in P1 cells, cholesterol storage was more apparent in these cells compared to P2 (Figure 1F). Similar increases in cholesterol accumulation were also noted in NgBR+/- mouse embryonic fibroblasts [6]. Together these findings reinforce the idea that cellular phenotypes occur in *NUS1* heterozygotes due to haploinsufficiency.

To more broadly assess an impact on lysosomal function in patient cells, the activity of multiple glycosidases was profiled. Acid-ß-glucosidase and ß-hexosaminidase activity was reduced in both the P1 and P2 fibroblasts but the activity of ß-galactosidase and ß-glucuronidase was either unaffected or slightly elevated (Figure 1G). It is not clear why acid-ß-glucosidase and ß-hexosaminidase activity is selectively reduced, but may reflect NgBR's ability to interact with and stabilize additional lysosomal proteins besides NPC2. For acid-ß-glucosidase, this reduction may also relate to impaired trafficking to the lysosome via a pathway distinct from the other soluble hydrolases [20-22]. Together, these data demonstrate that *de novo* loss-of-function variants in *NUS1* cause multiple lysosomal defects in patient cells.

The observed/expected (o/e) constraint score for *NUS1* generated by gnomAD is 0 with a 90% confidence interval of 0–0.25 indicating that haploinsufficiency of this gene is not tolerated [23]. While this supports haploinsufficiency as a pathogenic mechanism, we next aimed to formally rule out dominant negative effects as the basis for the cellular phenotypes. WT *NUS1* DNA or *NUS1* DNA bearing the c.734G>T (p.Gly245Val) variant in P1 were overexpressed in HeLa cells and glycosylation and cholesterol accumulation were assessed (Supplemental Figure 4). As a transfection control, a pcDNA3.1 construct expressing GFP was also utilized. Transfection of both *NUS1* DNA vectors caused robust expression of NUS1 protein in the cells (Supplemental Figure 4A). Although a decrease in the steady-state level of the NPC2 protein was noted in both the WT and Gly245Val overexpressing cells, this is likely a function of transfection, as the GFP construct produced comparable decreases. Notably, neither WT or p.Gly245Val NgBR overexpression in HeLa cells generated any intralysosomal cholesterol storage (Supplemental Figure 4B). In addition, no detectable impact on glycoprotein glycosylation was observed in HeLa cells overexpressing WT and Gly245Val NgBR protein, as judged by ICAM1 and LAMP2 Western blot in transfected cells (Supplemental Figure 4C). Together, these data support intolerance of this gene to loss-of-function variants and haploinsufficiency as a pathogenic mechanism.

Author Manuscript Author Manuscript Author Manuscript Author Manuscript

Zebrafish-based functional studies-

Western blot analyses of NgBR in zebrafish embryos 1-5 days post-fertilization (dpf) show the full length protein is abundant in early development (Figure 2A). Several developmentally regulated lower molecular weight forms, possibly resulting from alternative protein processing, were noted. To ask whether *NUS1* haploinsufficiency explains the clinical features of P1 and P2, we utilized an antisense morpholino to tune the knockdown of *nus1* expression in developing embryos. Dose-dependent reductions were achieved using 0.3-1.0μM morpholino, with 0.5μM consistently reducing steady-state levels ~50% from 1-6 dpf (Figure 2B,C). Although no overt physical phenotypes were noted in *nus1* morphants (Figure 2D), several differences in their motility and swimming behaviors emerged 4-5dpf. Unlike WT controls, which swim continuously, *nus1* morphants move erratically, stopping and starting often. To objectively measure differences between WT and morphant embryo swim behaviors we employed the Zebrabox, a behavioral analysis system that utilizes a high-speed camera housed in a sensory deprived chamber, to document and quantitate animal motility (Figure 2E). 5dpf embryos were placed one per well in 12-well dishes and sensory deprived in the enclosed recording chamber for 15 minutes. Swim behavior was subsequently recorded in 10-minute intervals. Using this method, swim behaviors of WT and *nus1* morphants were recorded once daily for 4 consecutive days. Traced paths of individual swim events revealed differences in swim speed, distance swam, the number of swim events initiated, and overall swim trajectory between WT and *nus1* morphants. Most notably, *nus1* morphants spent 40% more time swimming at high velocity (red paths) than WT embryos (Figure 2E). As a result, morphant embryos swam up to 40% further than WT embryos at each age analyzed. Although they spend more time swimming at high speed, *nus1* morphants also swim further at slow velocity (green paths). Importantly, in both categories, increased swim distances is associated with twice as many swim events. This indicates that *nus1* morphants move by initiating numerous short bursts of high-speed swim events. In combination with the pattern of traced swim paths, these data suggest morphant motility is uncoordinated compared to WT controls. WT embryos consistently propagate a slow continuous path that traverses the well whereas ~25% of *nus1*-deficient animals swim in a circle around the periphery of the well.

To ask if N-linked glycosylation is affected in *nus1* morphants, we utilized a transgenic zebrafish line that expresses a LAMP1-Cherry fusion protein under the control of a heat shock promoter (Figure 3A). WT and morphant transgenic embryos were heat shocked 4dpf, harvested 0.5-10h post-shock, and Lamp1-Cherry protein analyzed by Western blot with an anti-Cherry antibody (Figure 3B,C). These analyses show that while the same amount of Lamp1-Cherry protein is initially made (see 0.5h), by 3h post-shock its abundance is significantly higher in morphant embryos. Increased Lamp1-Cherry persists 10h post-shock. Accumulation of Lamp1-Cherry protein suggests lysosomal degradation may be impaired in *nus1* morphants. Although lower molecular weight products were noted, no definitive reduction in N-glycan occupancy was observed. Based on findings from patient fibroblasts we also addressed whether reductions in Npc2 and excess cholesterol could explain impaired Lamp1 proteolysis. Western blots for Npc2 show its abundance is decreased in morphant embryos 1-4 dpf (Figure 3D,E). Further, confocal analyses of embryos stained with filipin show reductions in Npc2 are associated with increased cholesterol (Figure 3G,H).

Author Manuscript Author Manuscript Author Manuscript Author Manuscript

Cholesterol accumulation was particularly evident in the hindbrains, spinal cords, and motor neurons of *nus1* morphants. Both motor neuron cell bodies and axonal projections were heavily stained by filipin in *nus1* morphants but not WT controls.

In order to ask whether cholesterol accumulation was associated with the movement phenotypes in *nus1* morphants, embryos were treated 4dpf with 2-hydroxypropyl-ß-cyclodextrin (ßCD). ßCD has been shown to facilitate cholesterol efflux from lysosomes reducing its accumulation in another Npc2-associated disorder, Niemann-Pick type C disease [24]. Confocal analyses of 7dpf filipin stained embryos (Figure 4A,B) show treatment with ßCD reduces cholesterol accumulation in all three *nus1*-affected tissues, including hindbrain, spinal cord, and motor neurons. Western blot analysis of Lamp1-Cherry further demonstrates that reducing cholesterol storage via ßCD treatment improves lysosomal function in *nus1* morphants (Figure 4C-E). This is evidenced by decreased accumulation of Lamp1-Cherry in ßCD treated morphants 5 and 10h post-shock.

Notably, *nus1*-depleted embryos showed significant improvement in several behavioral parameters following ßCD treatment (Figure 5). This was particularly evident when animals were given 2 doses (first at 4dpf and again at 6dpf). Most notably, ßCD treated *nus1* morphants exhibit increased coordination, with fewer animals swimming in circles on the edge of the dish (Figure 5B,C). Distance swam, swim speed, and numbers of swim events were also all significantly reduced in ßCD-treated morphants (Figure 5B-D). Collectively these findings suggest that *nus1*-dependent cholesterol accumulation is at least partially responsible for the motility phenotypes associated with *NUS1* haploinsufficiency.

Discussion:

The present work expands the phenotypic consequences associated with *NUS1* deficiency by demonstrating that *de novo* heterozygous loss-of-function variants in this gene are associated with seizures, ataxia and movement phenotypes in affected individuals. We provide functional evidence that patient fibroblasts exhibit a spectrum of lysosomal defects, most clearly manifested by lower abundance of the lysosomal cholesterol efflux protein, NPC2, and accumulation of free cholesterol in this organelle. Furthermore, we establish in zebrafish that a comparable reduction in *nus1* expression is sufficient to cause similar movement phenotypes that correlate with cholesterol accumulation in the brain and neuromuscular system. These phenotypes can be partially restored by treatment with 2-hydroxypropyl-ß-cyclodextrin, a chemical facilitator of cholesterol efflux from lysosomes. These findings indicate that at least some of the movement issues in human patients may be related to cholesterol accumulation in neuronal cells, and that therapies being developed for Niemann-Pick disease may be applicable to patients with *NUS1* variants. Our results provide insight into the mechanistic basis for the movement phenotypes associated with loss-of-function alleles in this gene.

Our results in zebrafish embryos show abundant cholesterol storage in the brain and neuromuscular system of zebrafish embryos at half maximal levels of the *nus1*/NgBR protein. Biochemical analysis of the *nus1*-deficient embryos did not reveal any obvious defects in N-glycosylation occupancy on the LAMP1 protein but did show an increase in its

Author Manuscript Author Manuscript Author Manuscript Author Manuscript

steady-state amount. This is suggestive of impaired proteolysis and/or turnover within lysosomes, which could arise from altered activity of resident proteases due to the accumulation of free cholesterol [25; 26]. Recent studies suggest limited lysosomal proteolysis plays a role in the pathogenesis of Parkinson's disease (PD) [27]. Loss of proteolytic capacity in lysosomes can impact processes such as mitophagy or other forms of autophagy, allowing failing organelles to accumulate and release toxic and reactive byproducts. While the movement phenotypes in our cohort don't overlap completely with PD, these data lend credence to the idea that neurons are particularly sensitive to disrupted lysosomal function [28]. This is further supported by the observation that the most notable cholesterol accumulation in the embryos is within the central nervous and neuromuscular systems. Despite reduced proteolytic capacity in the *nus1*-depleted zebrafish embryos and the cholesterol storage noted in patient fibroblasts, we observed only selective impairment in the function of lysosomal glycosidases, in particular, reduced activity of acid-ß-glucosidase and ß-hexosaminidase. This specificity raises the possibility that NgBR may be responsible for stabilizing other lysosomal proteins besides NPC2. Likewise, decreased activity of these glycosidases may have secondary effects on the turnover of glycolipids and calcium homeostasis [29]. Exploring this hypothesis, and the basis for the differences noted between the two patients, is a priority for future studies.

In light of the multiple functions carried out by NgBR, future studies will need to be aimed on defining whether and how the different functions of this protein contribute to the phenotypes seen in patients. Although alleviating cholesterol storage improved movement phenotypes of *nus1*-depleted embryos, it is unclear whether additional *nus1* functions (including its role at the NogoB receptor) also contribute. Since dolichol-based precursors are needed for other processes of other glycoconjugates such as the synthesis of GPI anchors, it is possible that impairment of these pathways is relevant. The sensitivity of the nervous system to alterations in many forms of glycosylation is well established, and could play a role in one or more of the phenotypes. Indeed, many proteins involved in neuronal development and function are heavily glycosylated, including voltage-gated ion channels, and can be impacted by limitations in dolichol-dependent precursors. In the event that deficits in glycosylation are more broadly implicated, increasing lipid flux away from *de novo* cholesterol biosynthesis and towards polyprenol/dolichol synthesis may be warranted. This can be done using inhibitors of squalene synthase, such as zaragozic acid, which would represent another possible therapeutic approach [30].

Supplementary Material

Refer to Web version on PubMed Central for supplementary material.

Acknowledgments

We acknowledge the patients and their families for their willingness to participate in this study. This work was supported by the Greenwood Genetic Center and grants from the National Institutes of Health (5R01-GM086524-11 to R.S. and H.F-S; AI108819 to M.B.C). We acknowledge the support of the Hazel and Bill Allin Aquaculture Facility housed at the Greenwood Genetic Center and thank the facility staff for their excellent animal care.

Author Manuscript Author Manuscript Author Manuscript Author Manuscript

References

1. Bar-El ML, Vankova P, Yeheskel A, Simhaev L, Engel H, Man P, Haitin Y, Giladi M Structural basis of heterotetrameric assembly and disease mutations in the human cis-prenyltransferase complex. Nat Commun. 2020;11, 5273. [PubMed: 33077723]
2. Edani BH, Grabinska KA, Zhang R, Park EJ, Siciliano B, Surmacz L, Ha Y, and Sessa WC. Structural elucidation of the cis-prenyltransferase NgBR/DHDDS complex reveals insights in regulation of protein glycosylation. PNAS. 2020;117, 20794–20802. [PubMed: 32817466]
3. Grabinska KA, Edani BH, Park EJ, Kraehling JR, and Sessa WC. A conserved C-terminal RXG motif in the NgBR subunit of cis-prenyltransferase is critical for prenyltransferase activity. J Biol Chem. 2017;292, 17351–17361. [PubMed: 28842490]
4. Grabinska KA, Park EJ, and Sessa WC. cis-Prenyltransferase: New Insights into Protein Glycosylation, Rubber Synthesis, and Human Diseases. J Biol Chem. 2016;291, 18582–18590. [PubMed: 27402831]
5. Harrison KD, Park EJ, Gao N, Kuo A, Rush JS, Waechter CJ, Lehrman MA, and Sessa WC. Nogo-B receptor is necessary for cellular dolichol biosynthesis and protein N-glycosylation. EMBO J. 2011;30, 2490–2500. [PubMed: 21572394]
6. Harrison KD, Miao RQ, Fernandez-Hernando C, Suarez Y, Davalos A, and Sessa WC. Nogo-B receptor stabilizes Niemann-Pick type C2 protein and regulates intracellular cholesterol trafficking. Cell Metabolism 2009;10, 208–218. [PubMed: 19723497]
7. Park EJ, Grabinska KA, Guan Z, and Sessa WC. NgBR is essential for endothelial cell glycosylation and vascular development. EMBO Reports. 2016 ;17, 167–177. [PubMed: 26755743]
8. Miao RQ, Gao Y, Harrison KD, Prendergast J, Acevedo LM, Yu J, Hu F, Strittmatter SM, and Sessa WC. Identification of a receptor necessary for Nogo-B stimulated chemotaxis and morphogenesis of endothelial cells. PNAS. 2006;103, 10997–11002. [PubMed: 16835300]
9. Teng RJ, Rana U, Afolayan AJ, Zhao B, Miao QR, and Konduri GG. Nogo-B receptor modulates angiogenesis response of pulmonary artery endothelial cells through eNOS coupling. Am J of Respiratory Cell and Molecular Biology. 2014;51, 169–177.
10. Park EJ, Grabinska KA, Guan Z, Stranecky V, Hartmannova H, Hodanova K, Baresova V, Sovova J, Jozsef L, Ondruskova N, et al. Mutation of Nogo-B receptor, a subunit of cis-prenyltransferase, causes a congenital disorder of glycosylation. Cell Metabolism. 2014;20, 448–457. [PubMed: 25066056]
11. Hamdan FF, Myers CT, Cossette P, Lemay P, Spiegelman D, Laporte AD, Nassif C, Diallo O, Monlong J, Cadieux-Dion M, et al. High Rate of Recurrent De Novo Mutations in Developmental and Epileptic Encephalopathies. AJHG. 2017;101, 664–685. [PubMed: 29100083]
12. Chen X, Xiao Y, Zhou M, Lin Y, Guo W, Huang S, Qiu J, Peng G, Mo M, Li Z, et al. Genetic analysis of NUS1 in Chinese patients with Parkinson's disease. Neurobiology of Aging. 2020;86, 202 e205–202 e206.
13. Guo JF, Zhang L, Li K, Mei JP, Xue J, Chen J, Tang X, Shen L, Jiang H, Chen C, et al. Coding mutations in NUS1 contribute to Parkinson's disease. PNAS. 2018;115, 11567–11572. [PubMed: 30348779]
14. Bustos BI, Bandres-Ciga S, Gibbs JR, Krainc D, Mencacci NE, Gan-Or Z, Lubbe SJ, and International Parkinson's Disease Genomics, C. Replication assessment of NUS1 variants in Parkinson's disease. Neurobiology of Aging. 2020; 11 13;S0197-4580(20)30389–4.
15. Yuan L, Chen X, Song Z, Le W, Zheng W, Liu X, and Deng H. Extended Study of NUS1 Gene Variants in Parkinson's Disease. Front Neurol. 2020;11, 583182. [PubMed: 33193043]
16. Araki K, Nakamura R, Ito D, Kato K, Iguchi Y, Sahashi K, Toyama M, Hamada K, Okamoto N, Wada Y, et al. NUS1 mutation in a family with epilepsy, cerebellar ataxia, and tremor. Epilepsy Res. 2020;164, 106371. [PubMed: 32485575]
17. Den K, Kudo Y, Kato M, Watanabe K, Doi H, Tanaka F, Oguni H, Miyatake S, Mizuguchi T, Takata A, et al. Recurrent NUS1 canonical splice donor site mutation in two unrelated individuals with epilepsy, myoclonus, ataxia and scoliosis - a case report. BMC Neurology. 2019;19, 253. [PubMed: 31656175]

Author Manuscript Author Manuscript Author Manuscript Author Manuscript

18. Szafranski P, Von Allmen GK, Graham BH, Wilfong AA, Kang SH, Ferreira JA, Upton SJ, Moeschler JB, Bi W, Rosenfeld JA, et al. 6q22.1 microdeletion and susceptibility to pediatric epilepsy. EJHG. 2015;23, 173–179. [PubMed: 24824130]
19. Wirth T, Tranchant C, Drouot N, Keren B, Mignot C, Cif L, Lefaucheur R, Lion-Francois L, Meneret A, Gras D, et al. Increased diagnostic yield in complex dystonia through exome sequencing. Parkinsonism & Related Disorders. 2020;74, 50–56. [PubMed: 32334381]
20. Reczek D, Schwake M, Schroder J, Hughes H, Blanz J, Jin X, Brondyk W, Van Patten S, Edmunds T, and Saftig P. LIMP-2 is a receptor for lysosomal mannose-6-phosphate-independent targeting of beta-glucocerebrosidase. Cell. 2007;131, 770–783. [PubMed: 18022370]
21. Zhao Y, Ren J, Padilla-Parra S, Fry EE, and Stuart DI. Lysosome sorting of beta-glucocerebrosidase by LIMP-2 is targeted by the mannose 6-phosphate receptor. Nat Commun. 2014;5, 4321. [PubMed: 25027712]
22. Zunke F, Andresen L, Wesseler S, Groth J, Arnold P, Rothaug M, Mazzulli JR, Krainc D, Blanz J, Saftig P, et al. Characterization of the complex formed by beta-glucocerebrosidase and the lysosomal integral membrane protein type-2. PNAS. 2016;113, 3791–3796. [PubMed: 27001828]
23. Lek M, Karczewski KJ, Minikel EV, Samocha KE, Banks E, Fennell T, O'Donnell-Luria AH, Ware JS, Hill AJ, Cummings BB, et al. Analysis of protein-coding genetic variation in 60,706 humans. Nature. 2016;536, 285–291. [PubMed: 27535533]
24. Ory DS, Ottinger EA, Farhat NY, King KA, Jiang X, Weissfeld L, Berry-Kravis E, Davidson CD, Bianconi S, Keener LA, et al. Intrathecal 2-hydroxypropyl-beta-cyclodextrin decreases neurological disease progression in Niemann-Pick disease, type C1: a non-randomised, open-label, phase 1-2 trial. Lancet. 2017;390, 1758–1768. [PubMed: 28803710]
25. Elrick MJ, and Lieberman AP. Autophagic dysfunction in a lysosomal storage disorder due to impaired proteolysis. Autophagy. 2013;9, 234–235. [PubMed: 23086309]
26. Elrick MJ, Yu T, Chung C, and Lieberman AP. Impaired proteolysis underlies autophagic dysfunction in Niemann-Pick type C disease. Human Molecular Genetics. 2012;21, 4876–4887. [PubMed: 22872701]
27. Nguyen M, Wong YC, Ysselstein D, Severino A, and Krainc D. Synaptic, Mitochondrial, and Lysosomal Dysfunction in Parkinson's Disease. Trends in Neurosciences. 2019;42, 140–149. [PubMed: 30509690]
28. Wong YC, Luk K, Purtell K, Burke Nanni S, Stoessl AJ, Trudeau LE, Yue Z, Krainc D, Oertel W, Obeso JA, et al. Neuronal vulnerability in Parkinson disease: Should the focus be on axons and synaptic terminals? Movement Disorders. 2019;34, 1406–1422. [PubMed: 31483900]
29. Lloyd-Evans E, Morgan AJ, He X, Smith DA, Elliot-Smith E, Sillence DJ, Churchill GC, Schuchman EH, Galione A, and Platt FM. Niemann-Pick disease type C1 is a sphingosine storage disease that causes deregulation of lysosomal calcium. Nat Med. 2008;14, 1247–1255. [PubMed: 18953351]
30. Haeuptle MA, Welti M, Troxler H, Hulsmeier AJ, Imbach T, and Hennet T. Improvement of dolichol-linked oligosaccharide biosynthesis by the squalene synthase inhibitor zaragozic acid. J Biol Chem. 2011;286, 6085–6091. [PubMed: 21183681]

Author Manuscript Author Manuscript Author Manuscript Author Manuscript

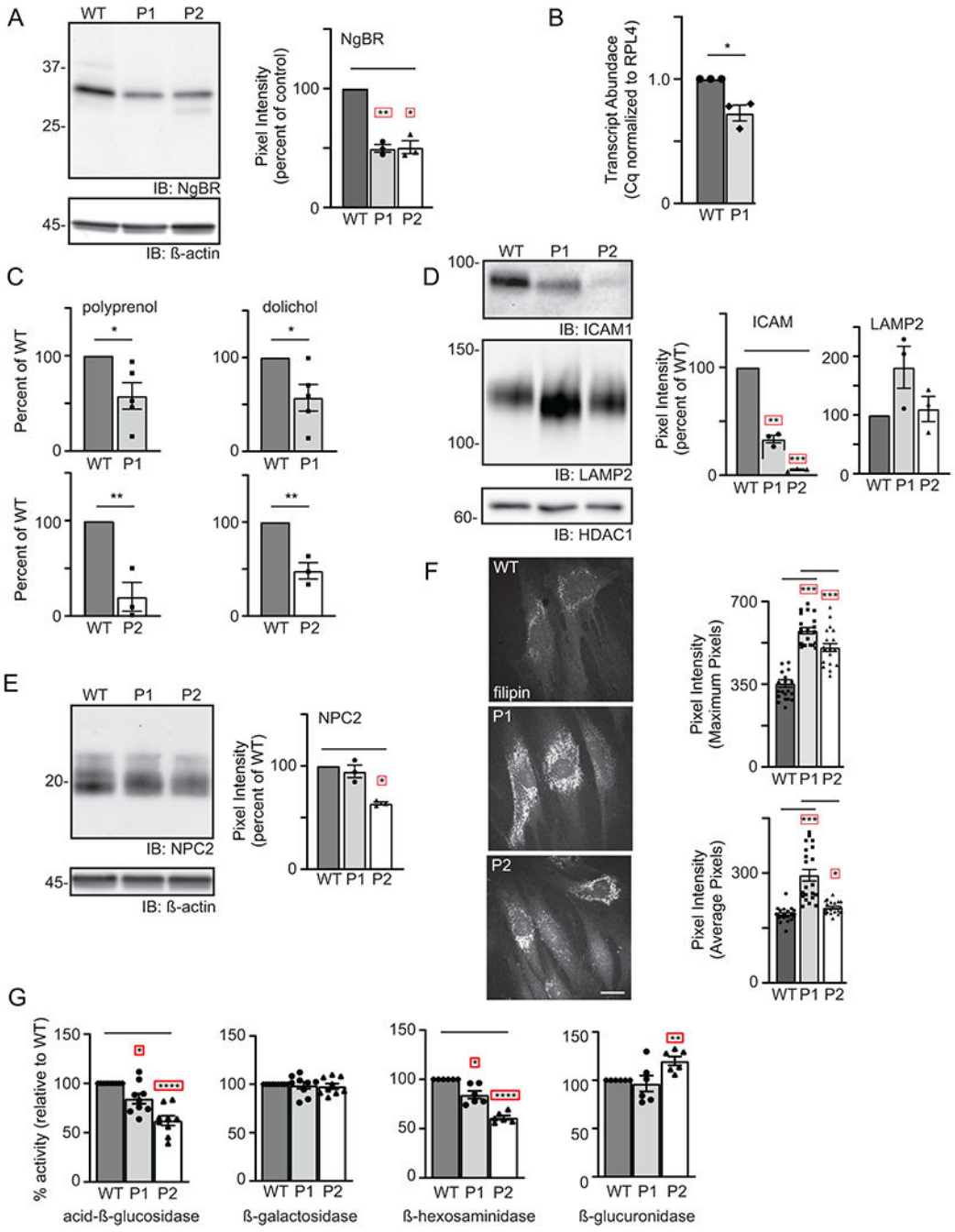

Figure 1: *De novo NUS1* variants cause a spectrum of lysosomal defects in patient cells.

(A) Representative Western blot for NgBR in WT and patient fibroblasts and quantitation of NgBR levels relative to ß-actin (n=3). Error=S.E.M. Statistical analysis was performed using a Dunnett's test. (B) Quantitative PCR analysis of *NUS1* transcripts in WT and P1 fibroblasts (n=3). The number of WT vs. variant alleles is shown. (C) Analysis of total dolichol and polyprenol levels in WT and patient fibroblasts. Analysis of the two patient lines (P1; n=5 and P2; n=3) were performed at different times using separate WT cells. Statistical analysis was performed using an unpaired Student's t test. (D) Representative

Author Manuscript Author Manuscript Author Manuscript Author Manuscript

Western blots for ICAM1 and LAMP2 in WT and patient fibroblasts and quantitation of protein levels relative to HDAC1 (n=3). Error=S.E.M. Statistical analysis was performed using a Dunnett's test. (E) Representative Western blot for NPC2 in WT and patient fibroblasts and quantitation of levels relative to ß-actin (n=3). Error=S.E.M. Statistical analysis was performed using a Dunnett's test. (F) Representative images of filipin-stained WT and patient fibroblasts and quantitation of pixel intensity in at least 40 different regions across 20 different cells. Error=S.E.M. Statistical analysis was performed using a Dunnett's test. Scale bar = 10μm. (G) Protein-normalized activity of acid-ß-glucosidase, ß-hexosaminidase, ß-glucuronidase and ß-galactosidase in WT and patient fibroblasts. Arbitrary fluorescence units are plotted. Statistical analysis was performed using a Dunnett's test. For all statistics *$p<0.05$, ** $p<0.01$, ***$p<0.001$. Red boxes indicate the additional correction (Dunnett's test) was applied for comparison to a single control group.

Author Manuscript Author Manuscript Author Manuscript Author Manuscript

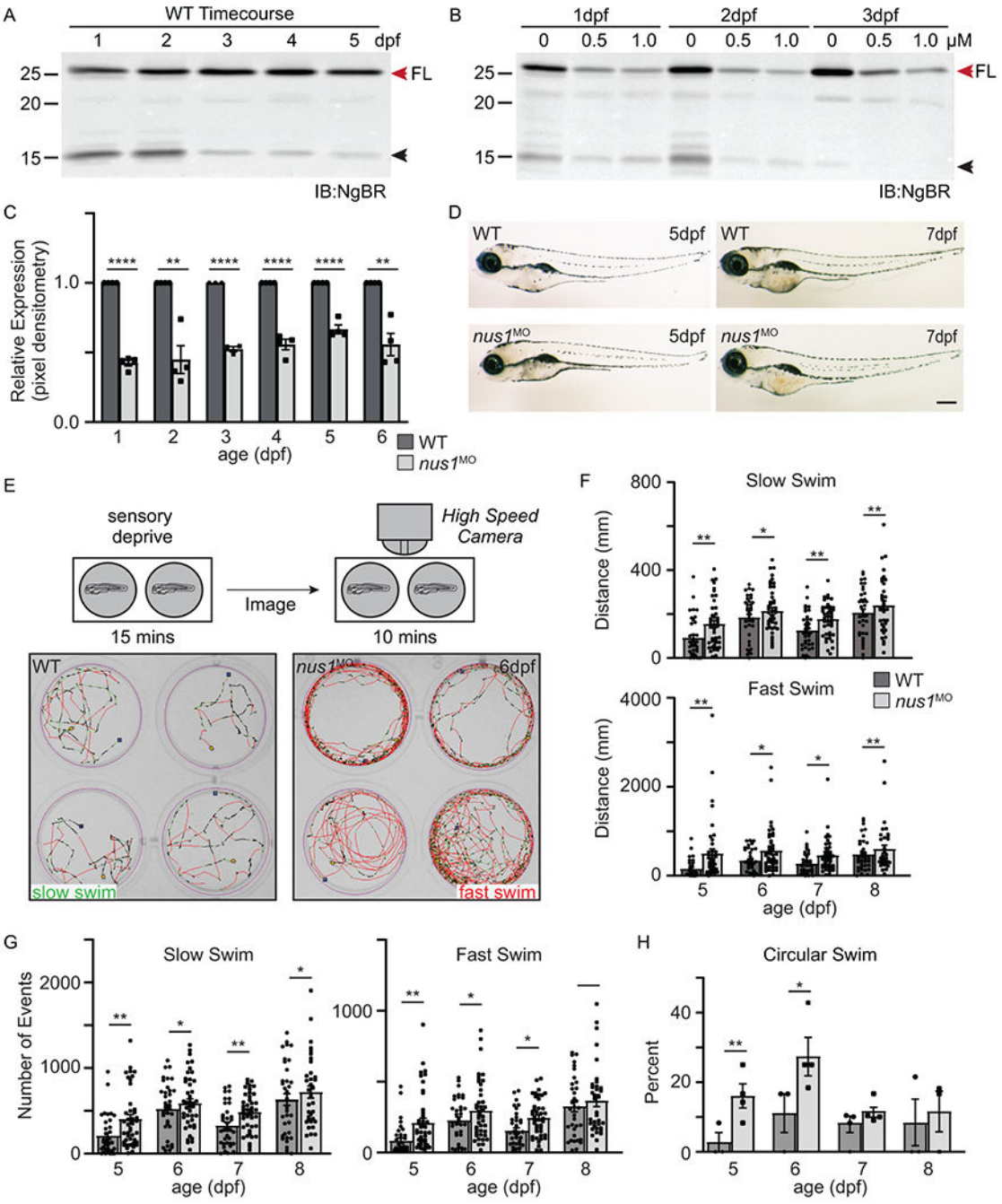

Figure 2: Reduction in *nus1* expression alters swim behavior of zebrafish embryos.

A) Western blots of 1-5dpf whole embryo lysates show NgBR is expressed during early development. Full length (FL) protein is indicated by a red arrowhead, as is a smaller processed piece. n=4 experimental replicates, 20 embryos per biological sample per experiment. B,C) Western blot show injection of 0.5 and 1.0 nM *nus1* morpholino reduces NgBR abundance ~50% in embryos 1-6dpf. n=4 experimental replicates, 20 embryos per biological sample per experiment. D) Bright field images of WT and *nus1* morphant (MO) embryos 5 and 7 dpf show no outward physical defects. n=100 embryos analyzed from 3

Author Manuscript Author Manuscript Author Manuscript Author Manuscript

experiments. Scale bar=100μm. E) Schematic describes workflow for Zebrabox analyses of embryo motility. Image of 4 representative wells are shown from one plate containing WT and *nus1* morphants. Traced swim patterns indicate the total path swam by the embryo, as well as swim speed. Red lines indicate a high velocity (fast) swim, while green lines indicate lower velocity (slow) swim. Images show *nus1* morphants spend more time swimming at higher velocity than WT, often swimming in a circle around the well. F) Graphs summarizing the distance swam by an individual embryo (one dot) while at the fast or slow speed from 5-8 dpf. G) Graphs illustrate the number of new swim events initiated by an individual fish (one dot) while at the slow or fast swim speed from 5-8 dpf. H) Graphs illustrate the percent of total embryos in 4-5 experiments that exclusively swim in a circle at the edge of the well. n=50-100 embryos. For all quantitation: n= 50-75 embryos over 4-6 independent experiments. Error= S.E.M., significance calculated by the student's t-test where *p<0.05, **p<0.01, ***p<0.001, ****p<0.0001.

Author Manuscript Author Manuscript Author Manuscript Author Manuscript

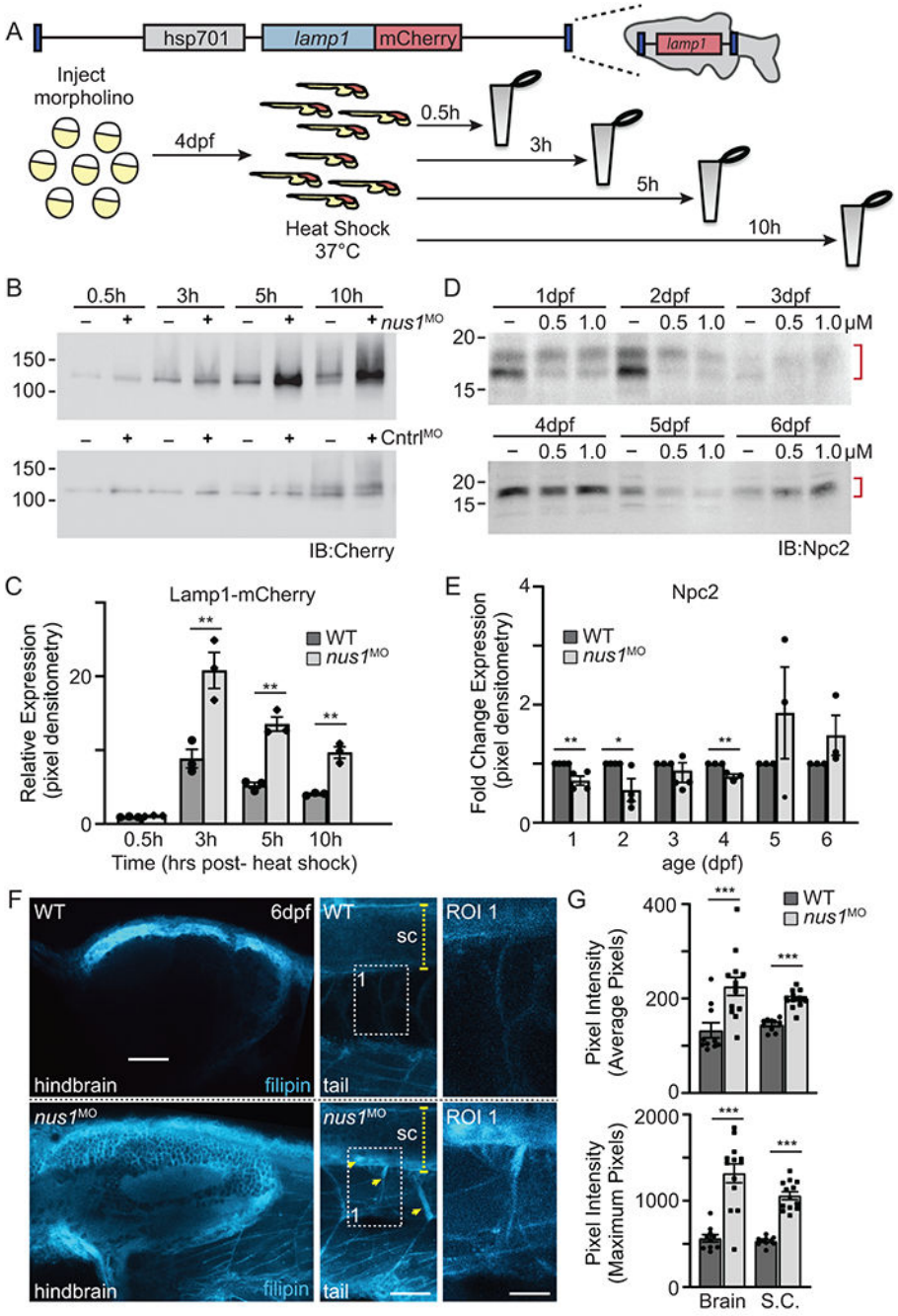

Figure 3: *nus1* morphants exhibit impaired lysosomal function and cholesterol accumulation.

A) Schematic illustrates transgene in zebrafish genome and the workflow for analyzing Lamp1 in WT and *nus1* morphant embryos. As shown, the transgene encodes a fusion between *lamp1* and monomeric Cherry (mCherry); expression is controlled by the heat shock promoter (hsp701). B,C) Western blot analysis and graphic quantitation of Lamp1 over a time course (0.5-10h) following heat shock induction of its expression show while similar amounts of Lamp1-mCherry are made post-heat shock, protein accumulates in *nus1* morphants. D,E) Western blot analysis and graphic quantitation of Npc2 abundance in WT

Author Manuscript Author Manuscript Author Manuscript Author Manuscript

and morphants (using either 0.5 or 1.0 μM morpholino) from 1-6dpf. Red bracket indicate Npc2 doublet; both bands included in the quantitation of relative abundance. For all graphs: n=3 experiments, with 25 embryo per sample per experiment. Error=S.E.M, significance calculated by the student's t-test where *p<0.05, **p<0.01. F) Confocal analyses of filipin stained WT and *nus1* morphant (MO) embryos 6dpf show cholesterol accumulation in the hindbrain, spinal cord (sc), and motor axons of morphant embryo tails. Yellow arrowheads highlight motor neuron cell bodies in ventral spinal cord and their associated axonal projections. Boxed region represents a region of interest (ROI) magnified in the right panel. Scale bars = 50 and 25 μM, respectively. G) Graph represents quantitation of the average and maximum pixel intensities from the hindbrains, spinal cords, and axons of 10-15 embryos from n=3 independent experiments. Error=S.E.M, significance calculated by the student's t-test where ***p<0.001.

Author Manuscript Author Manuscript Author Manuscript Author Manuscript

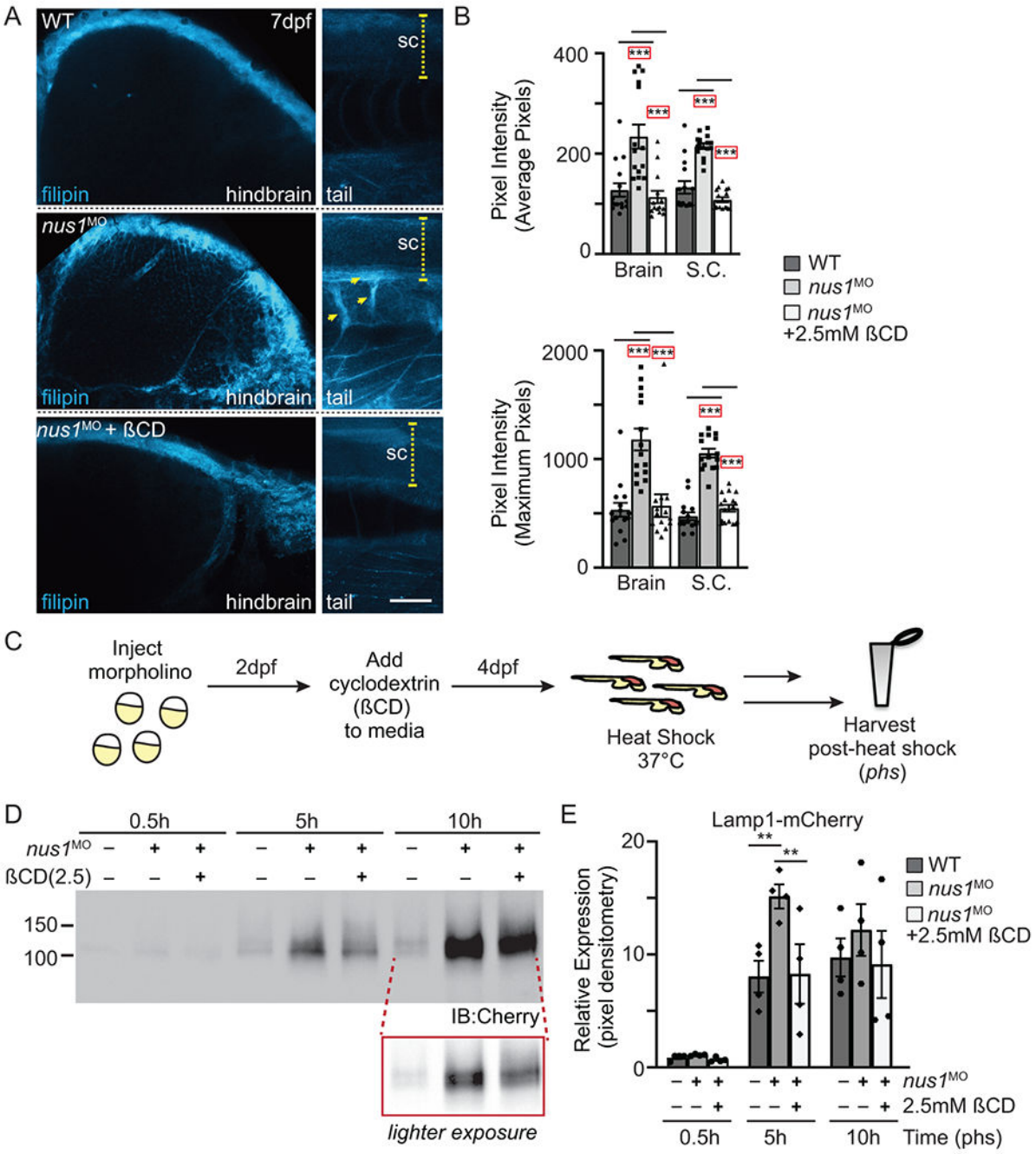

Figure 4: Treatment with ßCD reduces cholesterol accumulation and restores lysosomal function.

A) Confocal analyses of filipin stained WT, *nus1* morphant (MO), and ßCD treated *nus1* morphant embryos show reduced cholesterol accumulation in the hindbrain, spinal cord (sc), and motor axons of morphant embryos 7dpf. Yellow arrowheads highlight axonal projections motor neurons in ventral spinal cords of *nus1* morphants, which are not detected with filipin staining in either WT or ßCD treated embryos. Scale bars =50μM. B) Graph represents quantitation of pixel the average and maximum intensities from hindbrain, spinal cords, and axons of 15 embryos from n=3 experiments. Error=S.E.M, significance calculated

Author Manuscript Author Manuscript Author Manuscript Author Manuscript

by the student's t-test where ***p<0.001. C) Schematic illustrates workflow for analysis of Lamp1 expression following ßCD treatment. D,E) Western blot analysis and graphic quantitation of Lamp1 abundance (0.5-10h following heat shock induction of its expression) show Lamp1 accumulation is alleviated in *nus1* morphants treated with 2.5 mM ßCD. n=4 independent experiments with 25 embryos per sample per experiment. Error=S.E.M, significance calculated by the student's t-test where *p<0.05, **p<0.01.

Author Manuscript
Author Manuscript
Author Manuscript
Author Manuscript

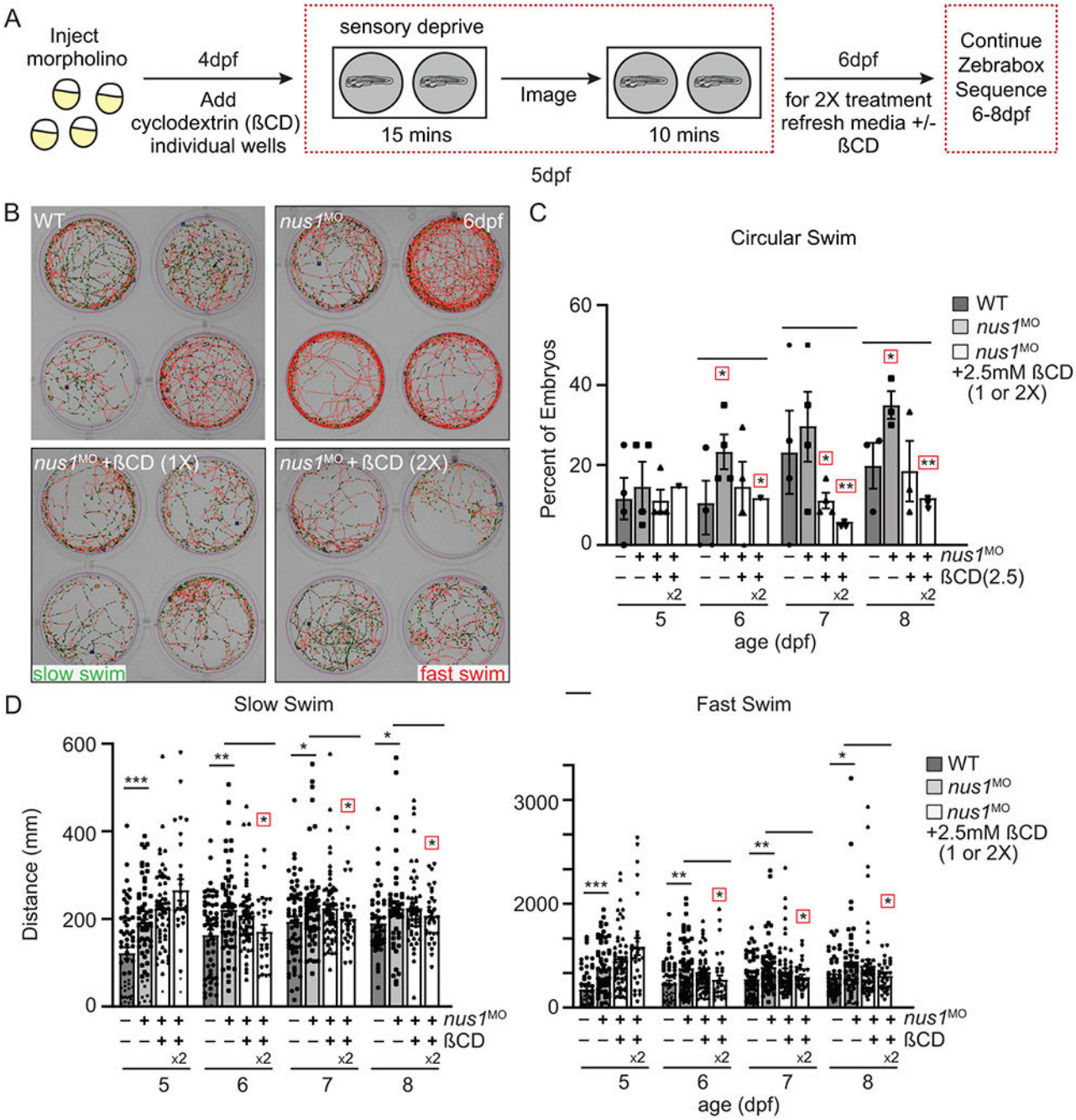

Figure 5: Lowering cholesterol accumulation improves swim behaviors in *nus1* morphant embryos.

A) Schematic illustrates workflow for Zebrabox analyses of embryo motility following ßCD treatment. B) Images show 4 representative wells from 12 well plates containing WT, *nus1* morphant, or nus1 morphant embryos treated 1 or 2x with 2.5mM ßCD. Traced swim patterns indicate the total path swam by the embryo, as well as swim speed. Red lines indicate a high velocity (fast) swim, while green lines indicate lower velocity (slow) swim. Images show treating *nus1* morphants with ßCD reduces both their swim speed and the tendency to swim in a circle around the well. C) Graph showing percent of total embryos

Author Manuscript Author Manuscript Author Manuscript Author Manuscript

swimming exclusively in a circle. D) Graph showing distance swam by an individual embryo (black dot) at slow and fast swim speeds 5-8dpf. Data show that treating *nus1* morphants with ßCD twice significantly reduces swim distance, restoring WT-like distances. For all graphs: n=3 experiments, with >25 embryos per "genotype" per condition. Error=S.E.M, significance calculated by the Dunnett's test where correction for a single control sample was applied. *p<0.05, **p<0.01. ***p<0.0001. Red boxes indicate an additional correction (Dunnett's test) was applied for comparison to a single control group.